JISSE
ISSN: 2636-4425

Journal of International Society for Science and Engineering
Vol. 6, No. 1, 18-25 (2024)

JISSE
E-ISSN:2682-3438

Computational Analysis of Dielectric Barrier Discharge Plasma Actuator Impact on Airfoil Characteristics

Deyaa N. Elshebiny[1], Kamal M. Ahmed[2], Amr A. Elfeky [3]*

[1] *Aerospace Engineering Department, Faculty of Engineering, Cairo University, Giza 12613, Egypt.*

[2] *Plasma and Nuclear Fusion Department, Nuclear Research Center, Egyptian Atomic Energy Authority, 13759, Cairo, Egypt.*

[3] *Mechanical Engineering Department, National Research Centre, Dokki, Cairo, Egypt.*

ARTICLE INFO

Article history:
Received: 30-07-2024
Accepted: 06-08-2024
Online: 14-08-2024

Keywords:
DBD Actuator,
Flow Separation,
NACA 0012 Airfoil,
Lift Coefficient
Drag Coefficient.

ABSTRACT

In recent years, Plasma actuators have strengthened the ability to control flows in creative manners leading to improvements in lift, drag reduction, and aerodynamic efficiency. These advancements could result in safe, more effective, and quiet aircraft. A numerical investigation is performed to determine the influence of Dielectric barrier Discharge (DBD) plasma on the flow properties of NACA 0012 airfoil at low Reynolds numbers, considering various angles of attack. The modified baseline airfoil was examined at three applied voltages 6.85 kV, 8.38 kV, and 11.45 kV at constant frequency. The results demonstrated that, when compared to the baseline airfoil, the DBD plasma actuator delays the trailing edge flow separation. Moreover, at 11.45 kV, the flow maintains attached to the airfoil at an angle of 20º and entirely eliminating the flow separation. Furthermore, the DBD airfoil significantly rising the lift coefficients while reducing the drag coefficients.

1. Introduction

Flow control is essential in aeronautical applications since it is needed for delaying or eliminating flow transitions, improving lift forces, and reducing drag forces. Flow control is usually classified into two categories: passive and active flow control. Passive control operates without the need for an external energy source, whereas active control needs external input energy. Dielectric barrier discharge (DBD) plasma actuators are a preferable approach to active flow control owing to their small size, low weight, durability, minimum power needs, and quick responses when activated [1-6]. The DBD plasma actuators are beneficial in several aerodynamics domains as they assist in controlling boundary layer flows [7,8], reducing noise [9,10], and enhancing fluid flow across the airfoil by postponing the separation point [11,12]. In DBD plasma actuator, two parallel asymmetrical electrodes, namely the exposed and the enclosed electrodes, are linked to a high-voltage power supply, typically 5-40 kV with a frequency of 1-20 kHz. These electrodes are isolated by a dielectric insulating sheet, which is typically made of materials such as Teflon or Kapton.

When a high-voltage power source is supplied to the electrodes and overcomes the breakdown electric field threshold, a non-thermal plasma is formed downstream of the exposed electrode on the dielectric interface. This plasma is composed of partly ionized air and does not significantly increase the temperature. The neutral fluid particles are subjected to collisions with moving ions when ionized air exists in the electric fields created by the two asymmetrical electrodes. This creates a body force that causes the boundary layer fluid particles to gain velocity, which speeds up the airflow and allows it to reattach with the surfaces [13–15]. Fig.1 depicts a schematic illustration of this phenomenon. The body forces generated by this plasma accelerate the airflow close to the plasma area, which is parallel to the dielectric surface, and transmits momentum to the fluid particles in the boundary layers. There are numerous applications for the DBD plasma actuator in aerodynamics Due to its ability to reduce noise [9,10] and delay the separation point [14,15]. Numerous investigations [16–18] examined the effects of a dielectric layer, supply voltage, frequency, electrode design, and gap spacing between them on the efficiencies of the plasma actuators. The flow control separation utilizing a DBD plasma actuator across a range of airfoil profiles, and flow visualization

* Amr El-Feky, Mechanical Engineering Department, National Research Centre, Cairo, Egypt, +201066805995, amr.elfeky@gmail.com

have been the subjects of numerous experimental studies [19, 20]. Several studies conducted smoke upstream of the airfoil in the wind tunnel [19], while others applied particle image velocimeters (PIV) to examine the ionic winds produced by the plasma [20–22]. Two methodologies were found in the literature to model the plasma actuators: the first principles-based models, and phenomenological (simplified) models. Consequently, the first principles-based models [27–30] are quite accurate when it comes to capturing plasma physics and near-wall physics. However, the phenomenological models [31–48] have gained much attention to model plasmas due to the ease of their modeling and execution. The goal of the current numerical simulation is to ascertain how the DBD plasma actuator affects the properties of the airfoil and the control of flow separation at various applied voltage values.

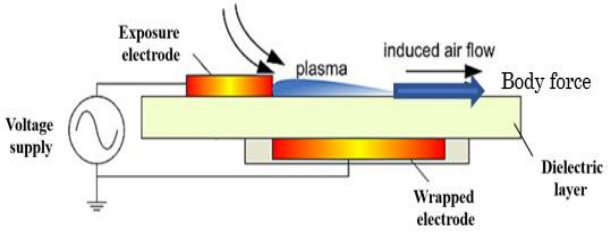

Figure 1. A schematic diagram of a DBD plasma actuator

This study concentrates on the numerical simulation of flow separation controlling above an airfoil designed to fit with a DBD plasma actuator via ANSYS Fluent software, which is a kind of plasma actuator that generates an electric field. The characteristics of plasma actuators, as well as the design of the actuators and the angles of attack, are adapted in order to examine their impacts.

2. DBD plasma actuator mathematical model

The mathematical model employed in this work to simulate the impacts of plasma actuators was created by Porter, et al. [49]. They suggested a linear fit between body force per unit length and the applied voltage at a fixed input frequency as shown in Fig. 2. The relation between body force and applied voltage can be correlated in equation (1). To model simplifying, the plasma region is assumed to be a rectangular region downstream exposed electrode as shown in Fig. 3.

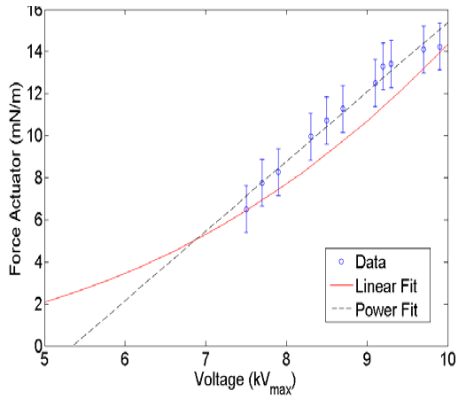

Figure 2. Average body force per meter of plasma at a constant forcing frequency of 5 kHz [49].

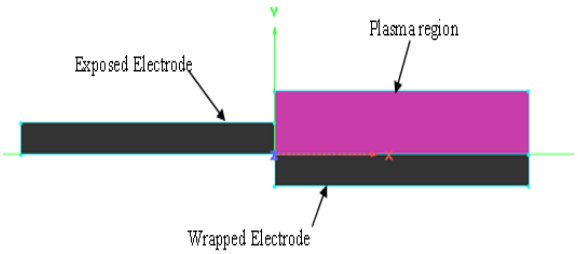

Figure 3. Plasma region as a rectangular domain approach

$$F_b = 3.26\,V - 17.32 \quad (1)$$

3. Numerical Discretization

3.1. Boundary Conditions and Grid System for DBD plasma actuator

A rectangular computational domain was constructed and electrodes and dielectric, with wall boundary conditions at DBD upstream and pressure outlet at DBD downstream as shown in Fig. 4.a and a wall boundary condition for the poles. The domain height is designed to be 1.5 m and extend 1.25 upstream and 2.75 downstream with pole dimensions presented in Fig. 4.b. Consequently, a structured mesh is utilized for system discretization. The grid system was designed to be dense near the electrodes, to capture the important physics at these positions with 427911 cells as seen in Fig. 5.a and zoomed view in Fig.5. b. In order to describe a plasma actuator, a user-defined function (UDF) is developed and compiled for the solver by adding a momentum source term to the proposed model. The length of the wrapped electrode and the plasma region were assumed to be the same length. The parameters of 10 mm in length and 0.1 mm in thickness were selected to represent the foil tape's relative size.

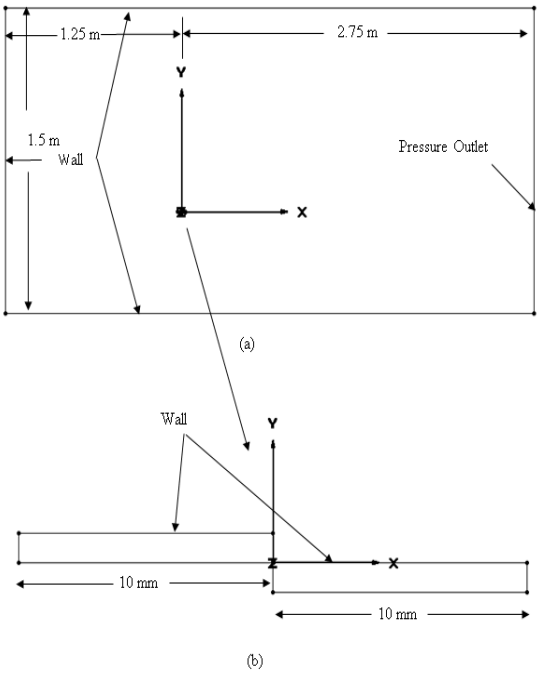

Figure 4. DBD actuator domain and Boundary conditions

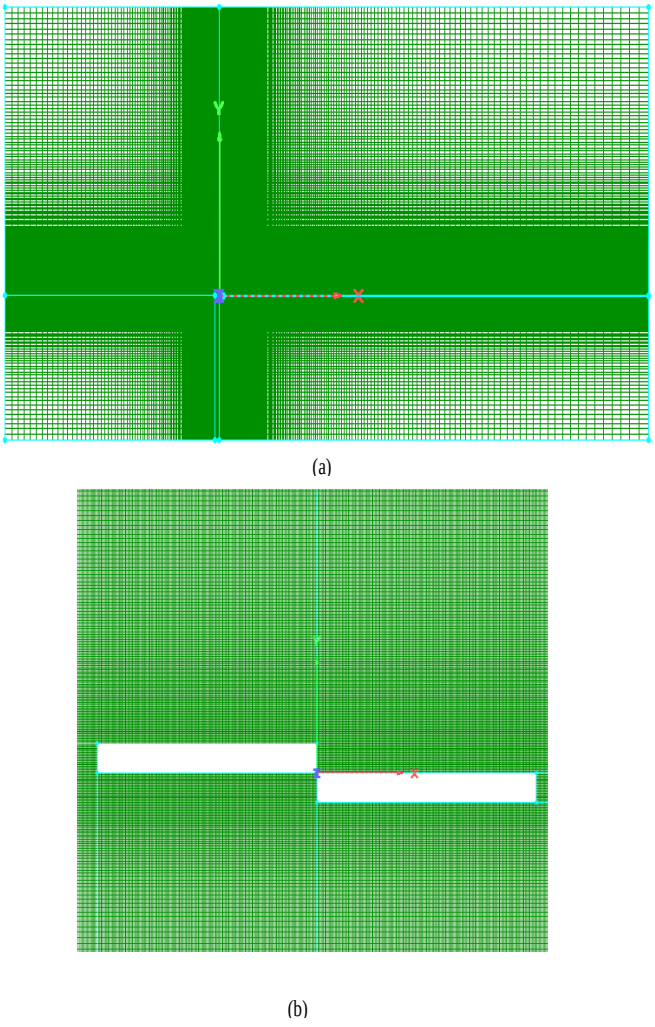

Figure 5. Grid System for computational domain and Poles

3.2. Numerical Set-up for airfoil DBD plasma

Numerical simulation is performed for a 2-D symmetrical NACA 0012 airfoil model, C domain type is used as a computational domain, and the domain is extended 15 of chord length upstream and 20 of chord length downstream with height 20 of a chord as seen in Fig. 6.a. The velocity inlet is defined as inlet boundary conditions, Pressure outlet at the outlet, symmetry boundary condition is defined for upper and lower sides, and wall boundary condition for the airfoil surfaces as seen in Fig. 6.b. For the grid system, a structured mesh is used for the entire domain as shown in Fig. 7.a grid and refined near the location of the actuator and airfoil to preserve Y+ less than 1 as shown in Fig.7.b with a total cell count of 343102 cells. The simulation is carried out on the airfoil at different angles of attack: 0, 4, 8, 10, 12, 14, 16, 18, and 20°, The DBD plasma actuator is placed at the upper surface at 0.05 cm away from the leading edge at applied voltage 6.85 kV, 8.38 kV, and 11.45 kV.

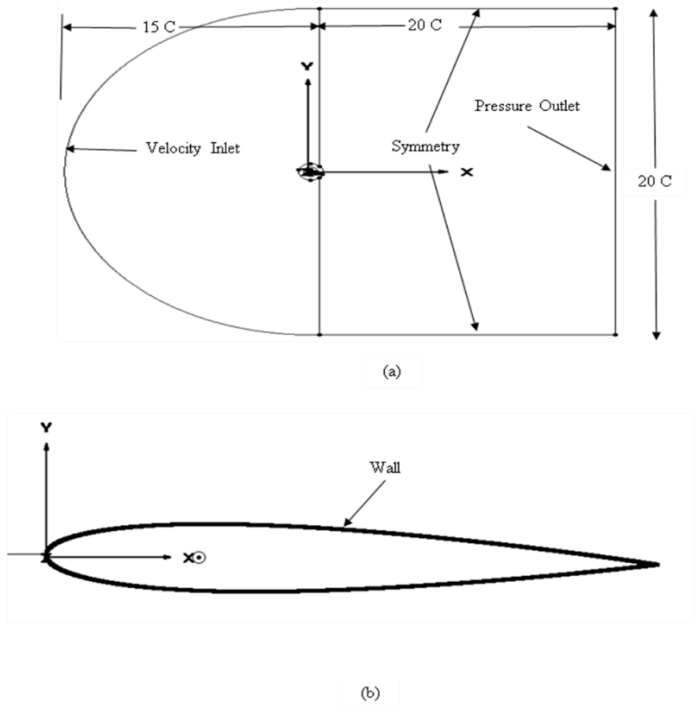

Figure 6. Model NACA 0012 airfoil with a plasma actuators Domain and Boundary Conditions

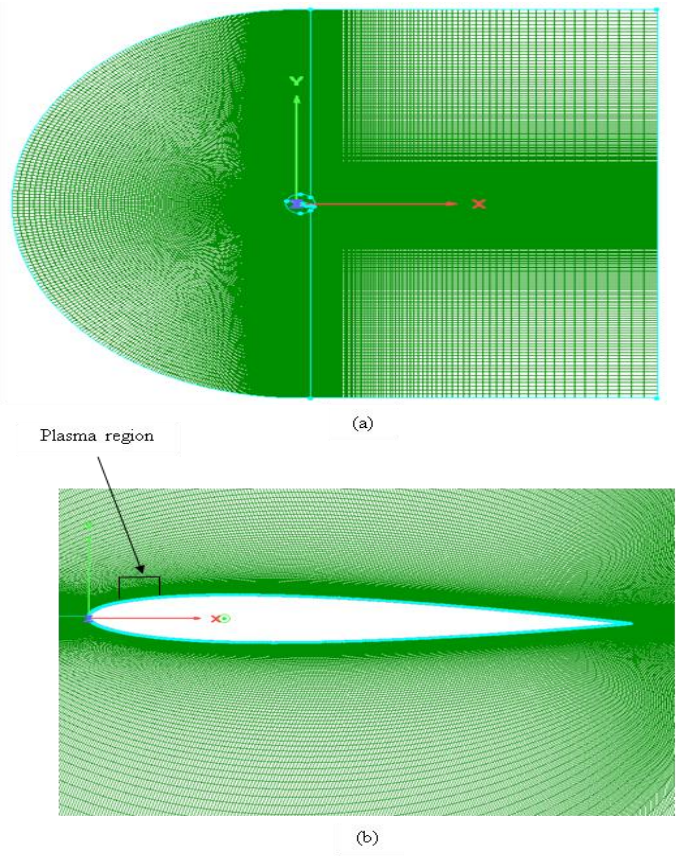

Figure 7. Grid System for airfoil equipped with DBD plasma actuator.

3.3. Model Validation

The experimental data of NACA 0012 [50] is chosen to validate the model, which had a chord of 60.10 cm and 91.44 cm span, tested in a low-turbulence wind tunnel. The tunnel sidewalls contain circular end plates with a diameter of 101.6 cm for positioning and attachment of the two-dimensional airfoil models. The stagnation temperature near ambient conditions is preserved using an air-to-water heat exchanger at 0.15 Mach and 3.94 x 106. Three turbulence models are tested in the current simulation namely Spalart-Allmaras, Kε Realizable, and Kω SST [51]. The results show that the Kω SST is the best model for predicting Lift and Drag Curves as shown in Fig.10; however, a difference is noticed in predicting the Drag coefficient in the stall regime.

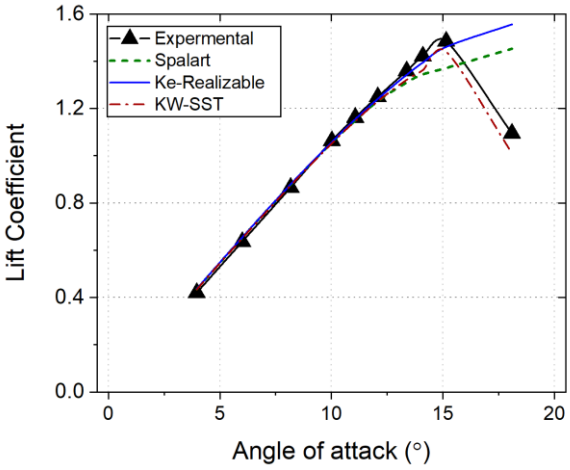

(a)

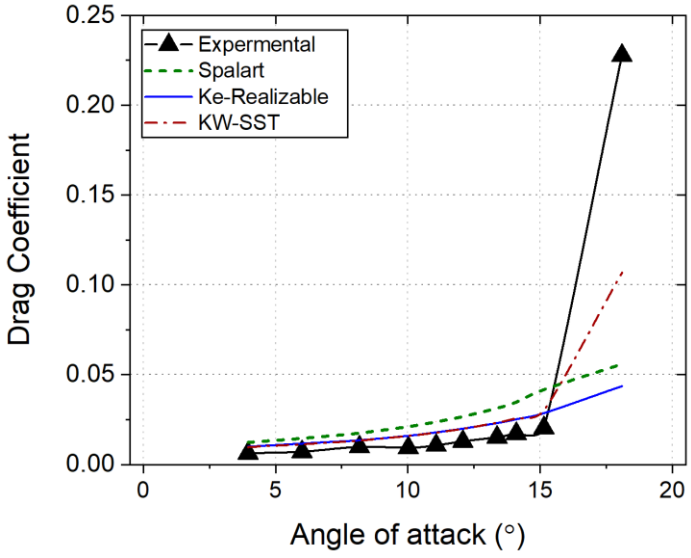

(b)

Figure 8. Comparison between the experimental data [50] and current simulation using Spalart-Allmaras, Kε realizable, and Kω SST turbulence models of (a) lift (b) drag coefficients

4. Results

4.1. DBD plasma actuator

The investigation begins with a parametric study of changing the body force f_b in the plasma region produced by the DBD actuator due to changing the supplied voltage at quiescent flow. DBD plasma actuator injects momentum into the flow and generates a body force. This body force can exert a direct momentum transfer to the fluid, causing flow acceleration. A wide variety of body force per unit meter at 500, 1000, 2000, 3000, 4000, 5000, 6000, 7000, 8000, 9000, 1000, and 11000 are examined. The velocity magnitude contours are plotted for the mentioned body forces per unit meter ranges as shown in Fig. 9 (a, b, c, d, e, f, g, h, i, j, k, and l), correspondingly. It is found that the induced ionic wind velocity in the plasma region downstream is proportionally increased with increasing the applied body force. Fig. 8 illustrates the velocity profiles, at the end of the wrapped electrode, of the DBD actuator downstream for various Body Forces per unit meter. At 11000 body force, the induced velocity approaches 11.8 m/s.

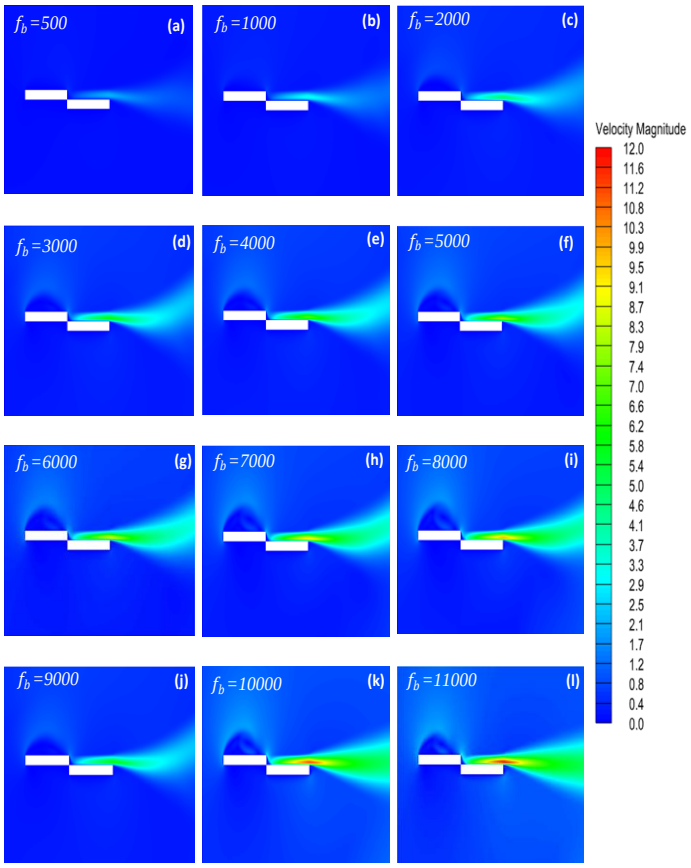

Figure 9. Velocity magnitude contours at DBD body force per meter 500, 1000, 2000, 3000, 4000, 5000, 6000, 7000, 8000, 9000, 1000, and 11000 (mN/m).

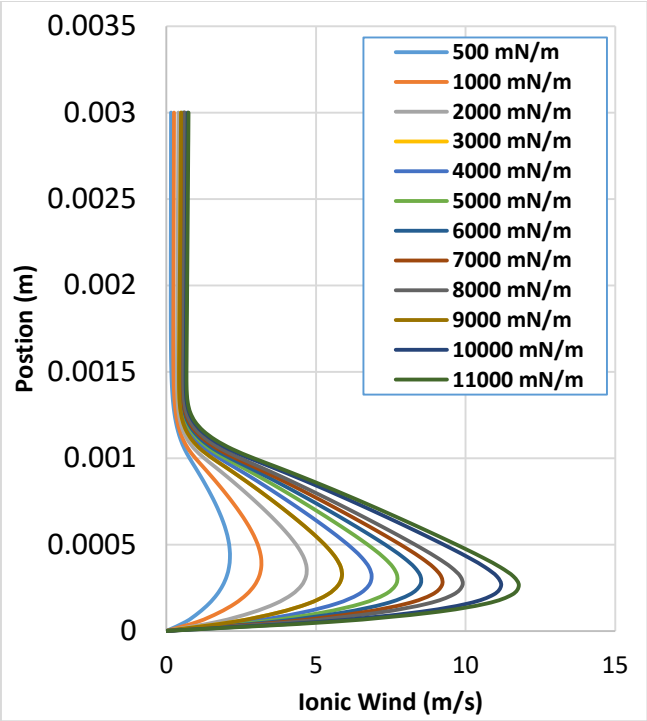

Figure 10. Velocity profiles above the DBD actuator for several Body Forces.

4.2. Base airfoil with no actuation

Velocity contours and streamlines around the baseline NACA 0012 airfoil with no actuation at angles of attack 10º, 12º, 14º, 16º, 18º and 20º as shown in Fig.11 a1, b1, c1, d1, e1, and f1 respectively. The flow remains attached to the airfoil until reaches to angle of 10º as shown in Fig.11.a1. At much higher angles of attacks trailing edge boundary layer separation occurs as seen in in Fig.11 b1, c1, d1, e1, and f1 and resulting in a sudden decrease in lift and an increase in drag as seen in Fig.13 a and b.

4.3. Airfoil DBD plasma

The second set of Fig. 11 demonstrates the DBD plasma airfoil in terms of velocity magnitude and stream lines at applied voltage = 6.85 kV. The flow remains attached to the upper surface of the base airfoil to 16º upstroke, as shown in Fig.11 a1, b1, c1, and d1. It is evident that the plasma actuator has the ability to significantly delay and shrink the separation region. It is noticed that at angles 18º and 20º shown in Fig.11 e1 and f1, the trailing edge separation occurs accompanied by a decrease in lift and increases in drag coefficients as shown in Fig.13 a and b. Figure 12 a, b, and c represent the streamline and velocity contours at applied voltage 6.85, 8.38, and 11.45 kV, respectively at 20º angle of attack. It is evident that when the applied voltage is raised, the lift coefficient increases, and the drag coefficient decreases, resulting in a decrease in flow separation. At 11.45 kV applied voltage, the flow separation is completely eliminated, as shown in Fig.11.d_1 with a significant increase in lift coefficient and decrease in Drag coefficient as shown in Fig. 13 a and b.

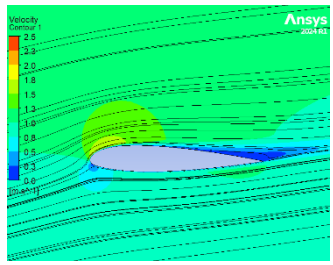

(a_1) α=10° (DBD Plasma Off)

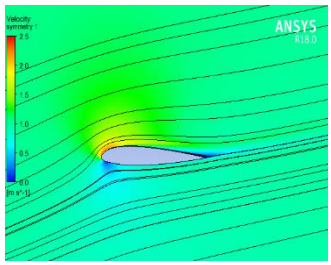

(a_2) α=10° (DBD Plasma On)

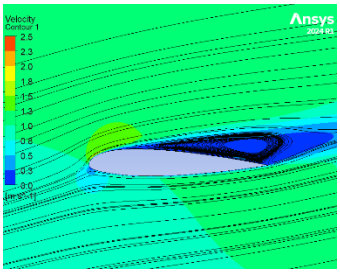

(b1) α=12° (DBD Plasma Off)

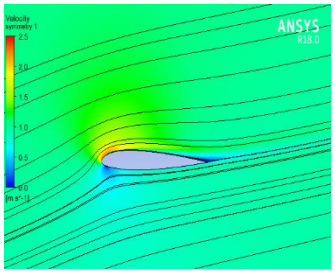

(b2) α=12° (DBD Plasma On)

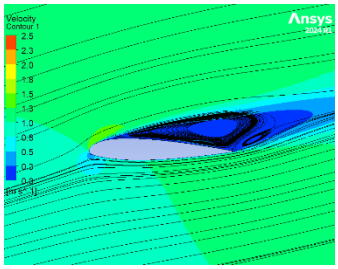

(c_1) α=14° (DBD Plasma Off)

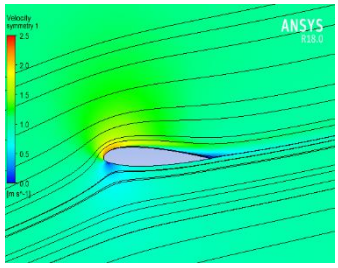

(c_2) α=14° (DBD Plasma On)

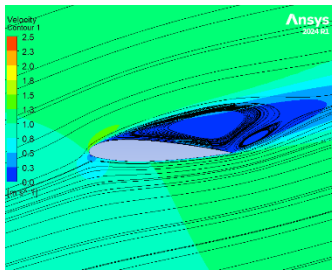

(d_1) α=16° (DBD Plasma Off)

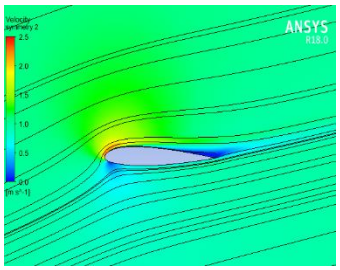

(d_2) α=16° (DBD Plasma On)

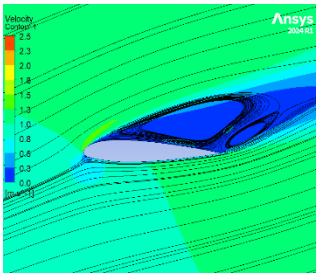

(e_1) α=18° (DBD Plasma Off)

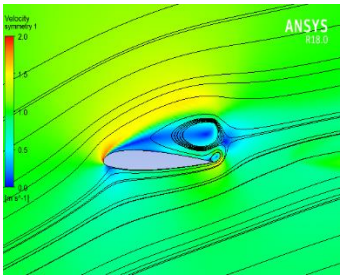

(e_2) α=18° (DBD Plasma On)

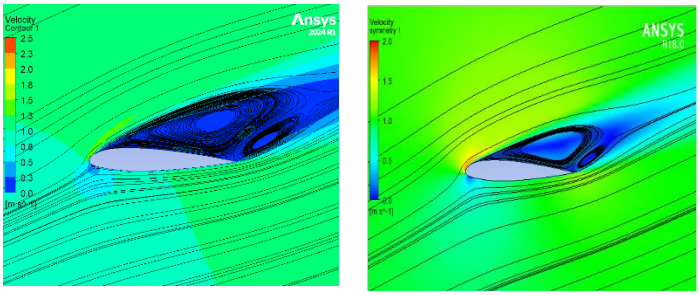

(f_1) α=20° (DBD Plasma Off) (f_2) α=20° (DBD Plasma On)

Figure 11. Streamlines around the plasma region in the case of 6.85 kV at angle of attack = (a) 14 (b) 16 (c) 18 (d) 20°.

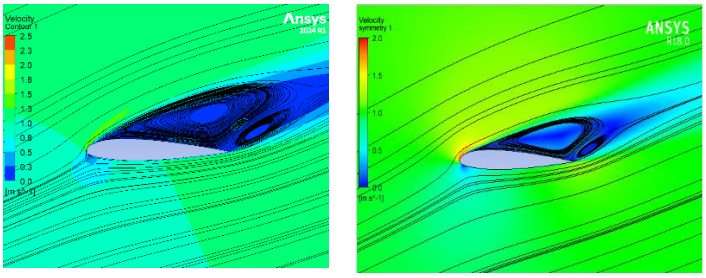

(a) α=20° (DBD Plasma Off) **(b)** α=20° (Applied Voltage 6.85 kV)

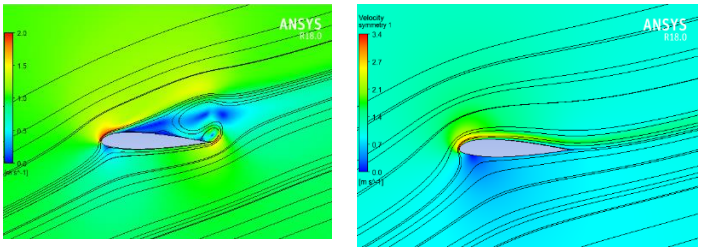

(b) α=20° (Applied Voltage 8.38 kV) **(b)** α=20° (Applied Voltage 11.45 kV)

Figure 12. Streamlines around the plasma region at an angle of attack 20º in the case of applied voltage (a) 6.85 kV (b) 8.38 kV (c) 11.45 kV

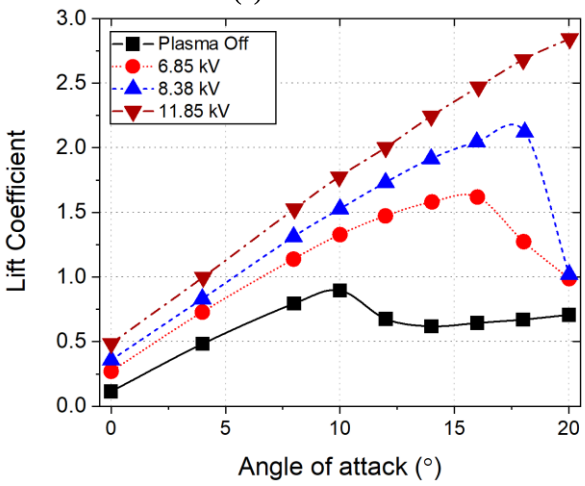

(a)

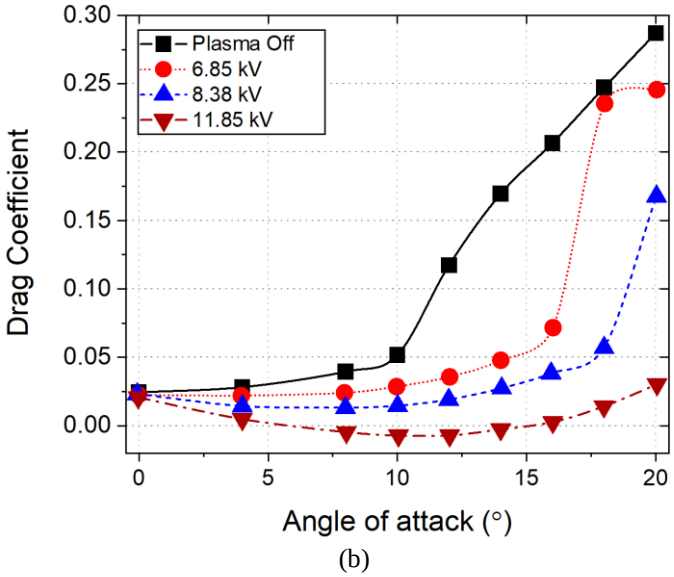

(b)

Figure 13. The (a) lift and (b) drag coefficients versus angle of attack at different supplied voltages of the DBD plasma actuator.

5. Conclusions

Recently, the DBD actuator is one of the most promising devices for effective flow control, especially in airfoils. Numerical simulation is performed to determine the effect of the DBD plasma actuator on airfoil characteristics at different values of applied voltages. The results indicate that increasing the supplied voltage results in an increase in lift coefficients as well as a reduction in drag coefficients and it is concluded that:

- The induced ionic wind velocity in the plasma region downstream is proportionally increased with increasing the applied body
- DBD plasma causes delay and shrinks the separation region over the upper surface of the airfoil.
- In the case of a deep stall regime, at 11.45 kV applied voltage, the flow separation is entirely eliminated combined with a substantial rise in lift coefficients and decrease in drag coefficients.

References

[1] Genç, M. S., Koca, K., Demir, H., & Açıkel, H. H. (2020). Traditional and New Types of Passive Flow Control Techniques to Pave the Way for High Maneuverability and Low Structural Weight for UAVs and MAVs. In Autonomous Vehicles. IntechOpen.

[2] Sotoudeh, F., Pourabidi, R., Mousavi, S. M., Goshtasbi-Rad, E., & Jeung, I. S. (2019). Hybrid passive-active control method of a swept shock wave-supersonic wake interaction. Acta Astronautica, 160, 509-518.

[3] Alber, J., Soto-Valle, R., Manolesos, M., Bartholomay, S., Nayeri, C. N., Schönlau, M., ... & Fortmann, J. (2020). Aerodynamic effects of Gurney flaps on the rotor blades of

a research wind turbine. Wind Energy Science, 5(4), 1645-1662.

[4] Gnani, F., Zare-Behtash, H., & Kontis, K. (2016). Pseudo-shock waves and their interactions in high-speed intakes. Progress in Aerospace Sciences, 82, 36-56.

[5] Kral, L. D. (2000). Active flow control technology. ASME Fluids Engineering Technical Brief.

[6] Kamali, R., Mousavi, S. M., & Binesh, A. R. (2015). Three dimensional CFD investigation of shock train structure in a supersonic nozzle. Acta Astronautica, 116, 56-67.

[7] Font, G. I. (2006). Boundary layer control with atmospheric plasma discharges. AIAA journal, 44(7), 1572-1578.

[8] Zoppini, G., Belan, M., Zanotti, A., Di Vinci, L., & Campanardi, G. (2020). Stall control by plasma actuators: Characterization along the airfoil span. Energies, 13(6), 1374.

[9] Wasala, S., Peng, S. H., Davidson, L., González-Gutiérrez, L., & Morán-Guerrero, A. (2019, September). Modelling of DBD plasma actuator for controlling noise from a tandem cylinders configuration. In INTER-NOISE and NOISE-CON Congress and Conference Proceedings (Vol. 259, No. 9, pp. 876-888). Institute of Noise Control Engineering.

[10] Hasheminejad, S. M., Chong, T. P., Lacagnina, G., Joseph, P., Kim, J. H., Choi, K. S., ... & Stalnov, O. (2020). On the manipulation of flow and acoustic fields of a blunt trailing edge aerofoil by serrated leading edges. The Journal of the Acoustical Society of America, 147(6), 3932-3947.

[11] Brandenburg, R. (2017). Dielectric barrier discharges: progress on plasma sources and on the understanding of regimes and single filaments. Plasma Sources Science and Technology, 26(5), 053001.

[12] Kogelschatz, U., Eliasson, B., & Egli, W. (1997). Dielectric-barrier discharges. Principle and applications. Le Journal de Physique IV, 7(C4), C4-47.

[13] Abdollahzadeh, M., Pascoa, J., & Oliveira, P. (2012). Numerical modeling of boundary layer control using dielectric barrier discharge. In MEFTE IV National Conference on Fluid Mechanics, Thermodynamics and Energy, Lisbon, LNEC, (May 28-29, 2012).

[14] Kesuma, M. D., Irwansyah, R., Julian, J., & Satyadharma, A. (2020). Flow Control with Multi-DBD Plasma Actuator on a Delta Wing. Evergreen, 7(4), 602-608.

[15] Singhal, A., Castañeda, D., Webb, N., & Samimy, M. (2018). Control of dynamic stall over a NACA 0015 airfoil using plasma actuators. AIAA Journal, 56(1), 78-89.

[16] Benard, N., & Moreau, E. (2012). Role of the electric waveform supplying a dielectric barrier discharge plasma actuator. Applied Physics Letters, 100(19), 193503.

[17] Forte, M., Jolibois, J., Pons, J., Moreau, E., Touchard, G., & Cazalens, M. (2007). Optimization of a dielectric barrier discharge actuator by stationary and non-stationary measurements of the induced flow velocity: application to airflow control. Experiments in fluids, 43(6), 917-928.

[18] Thomas, F. O., Corke, T. C., Iqbal, M., Kozlov, A., & Schatzman, D. (2009). Optimization of dielectric barrier discharge plasma actuators for active aerodynamic flow control. AIAA journal, 47(9), 2169-2178.

[19] Post, M. L., & Corke, T. C. (2006). Separation control using plasma actuators: dynamic stall vortex control on oscillating airfoil. AIAA journal, 44(12), 3125-3135.

[20] Benard, N., Braud, P., Jolibois, J., & Moreau, E. (2008, June). Airflow reattachment along a NACA 0015 airfoil by surfaces dielectric barrier discharge actuator: Time-resolved particle image velocimetry investigation. In 4th Flow Control Conference (p. 4202).

[21] Maden, I., Maduta, R., Kriegseis, J., Jakirlić, S., Schwarz, C., Grundmann, S., & Tropea, C. (2013). Experimental and computational study of the flow induced by a plasma actuator. International Journal of Heat and Fluid Flow, 41, 80-89.

[22] Kriegseis, J., Schwarz, C., Tropea, C. A., & Grundmann, S. (2013). Velocity-information-based force-term estimation of dielectric-barrier discharge plasma actuators. Journal of Physics D: Applied Physics, 46(5), 055202.

[23] Abdelraouf, H., Elmekawy, A. M. N., & Kassab, S. Z. (2020). Simulations of flow separation control numerically using different plasma actuator models. Alexandria Engineering Journal, 59(5), 3881-3896.

[24] Li, L., Lange, C. F., & Ma, Y. (2018). Association of design and computational fluid dynamics simulation intent in flow control product optimization. Proceedings of the Institution of Mechanical Engineers, Part B: Journal of Engineering Manufacture, 232(13), 2309-2322.

[25] Xie, L., Liang, H., Han, M., Niu, Z., Wei, B., Su, Z., & Tang, B. (2019). Experimental Study on Plasma Flow Control of Symmetric Flying Wing Based on Two Kinds of Scaling Models. Symmetry, 11(10), 1261.

[26] Rozeman, S. (2014). CFD study on performance of a DBD Plasma Actuated airfoil in an ultra-low Reynolds number flow. Report Internship University of Twente – ISAS/JAXA Internship.

[27] Riley, M.; Greenberg, K.; Hebner, G.; Drallos, P. Theoretical and experimental study of low-temperature, capacitively coupled, radio-frequency helium plasmas. J. Appl. Phys. 1994, 75, 2789–2798.

[28] Golubovskii, Y.B.; Maiorov, V.; Behnke, J.; Behnke, J. Modelling of the homogeneous barrier discharge in helium at atmospheric pressure. J. Phys. D Appl. Phys. 2002, 36, 39.

[29] Massines, F.; Rabehi, A.; Decomps, P.; Gadri, R.B.; Ségur, P.; Mayoux, C. Experimental and theoretical study of a glow discharge at atmospheric pressure controlled by dielectric barrier. J. Appl. Phys. 1998, 83, 2950–2957.

[30] Fiala, A.; Pitchford, L.; Boeuf, J. Two-dimensional, hybrid model of low-pressure glow discharges. Phys. Rev. E 1994, 49, 5607.

[31] Shyy, W.; Jayaraman, B.; Andersson, A. Modeling of glow discharge-induced fluid dynamics. J. Appl. Phys. 2002, 92, 6434–6443.

[32] Suzen, Y.; Huang, G. Simulations of flow separation control using plasma actuators. In Proceedings of the 44th AIAA Aerospace Sciences Meeting and Exhibit, Reno, Nevada, 9–12 January 2006; p. 877.

[33] Suzen, Y.; Huang, G.; Jacob, J.; Ashpis, D. Numerical simulations of plasma-based flow control applications. In Proceedings of the 35th AIAA Fluid Dynamics Conference and Exhibit, Toronto, ON, Canada, 6–9 June 2005; p. 4633.

[34] Roth, J.; Sherman, D.; Wilkinson, S. Boundary layer flow control with a one atmosphere uniform glow discharge surface plasma. In Proceedings of the 36th AIAA Aerospace Sciences Meeting and Exhibit, Reno, NV, USA, 12–15 January 1998; p. 328.

[35] Enloe, C.; McLaughlin, T.E.; Van Dyken, R.D.; Kachner, K.; Jumper, E.J.; Corke, T.C. Mechanisms and responses of a single dielectric barrier plasma actuator: Plasma morphology. AIAA J. 2004, 42, 589–594.

[36] Orlov, D.; Corke, T.; Patel, M. Electric circuit model for aerodynamic plasma actuator. In Proceedings of the 44th AIAA Aerospace Sciences Meeting and Exhibit, Reno, NV, USA, 9–12 January 2006; p. 1206.

[37] Khoshkhoo, R.; Jahangirian, A. Flow separation control over airfoils using DBD plasma body force. J. Braz. Soc. Mech. Sci. Eng. 2016, 38, 2345–2357.

[38] Gaitonde, D.; Visbal, M.; Roy, S. Control of flow past a wing section with plasma-based body forces. In Proceedings of the 36th AIAA Plasmadynamics and Lasers Conference, Toronto, ON, Canada, 6–9 June 2005; p. 5302.

[39] Yu, J.; Liu, H.; Wang, R.; Chen, F. Numerical study of the flow structures in flat plate and the wall-mounted hump induced by the unsteady DBD plasma. Plasma Sci. Technol. 2016, 19, 015502.

[40] Mushyam, A.; Rodrigues, F.; Pascoa, J. A plasma-fluid model for EHD flow in DBD actuators and experimental validation. Int. J. Numer. Methods Fluids 2019, 90, 115–139.

[41] Gang, L.; Chaoqun, N.; Yiming, L.; Junqiang, Z.; Yanji, X. Experimental investigation of flow separation control using dielectric barrier discharge plasma actuators. Plasma Sci. Technol. 2008, 10, 605.

[42] Rodrigues, F.; Mushyam, A.; Pascoa, J.; Trancossi, M. A new plasma actuator configuration for improved efficiency: The stair-shaped dielectric barrier discharge actuator. J. Phys. D Appl. Phys. 2019, 52, 385201.

[43] Corke, T.; Jumper, E.; Post, M.; Orlov, D.; McLaughlin, T. Application of weakly-ionized plasmas as wing flow-control devices. In Proceedings of the 40th AIAA Aerospace Sciences Meeting & Exhibit, Reno, NV, USA, 14–17 January 2002; p. 350.

[44] Rizzetta, D.P.; Visbal, M.R. Large-eddy simulation of plasma based turbulent boundary-layer separation control. AIAA J. 2010, 48, 2793–2810.

[45] Hasan, M.; Atkinson, M. Control of Flow Separation on a Hump Model Using a Dielectric Barrier Discharge Plasma Actuator. Early Career Tech. J. UAB Sch. Eng. Mech. Eng. 2019, 18.

[46] Ma, L.; Wang, X.; Zhu, J.; Kang, S. Effect of DBD plasma excitation characteristics on turbulent separation over a hump model. Plasma Sci. Technol. 2018, 20, 105503.

[47] He, C.; Corke, T.; Patel, M. Numerical and experimental analysis of plasma flow control over a hump model. In Proceedings of the 45th AIAA Aerospace Sciences Meeting and Exhibit, Reno, NV, USA, 8–11 January 2007; p. 935.

[48] Hasan, M., & Atkinson, M. (2020). Investigation of a Dielectric Barrier Discharge Plasma Actuator to Control Turbulent Boundary Layer Separation. Applied Sciences, 10(6), 1911.

[49] C. O. Porter., J. W. Baughn., T. E. McLaughlin, C. L. Enloe, and G. I. Font. Temporal Force Measurements on an Aerodynamic Plasma Actuator. 44th AIAA Aerospace Sciences Meeting and Exhibit 9 - 12 January 2006, Reno, Nevada.

[50] Charles L. Ladson., “Effects of Independent Variation of Mach and Reynolds Numbers on the Low-Speed Aerodynamic Characteristics of the NACA 0012 Airfoil Section," NASA National Aeronautics and Space Administration Scientific and Technical Information Division 1988

[51] ANSYS Fluent Theory Guide,” vol. 15317, no. November, pp. 724–746, 2013.